

Activation Energy of the Low-pH-Induced Lamellar to Bicontinuous Cubic Phase Transition in Dioleoylphosphatidylserine/Monoolein

メタデータ	言語: en 出版者: American Chemical Society 公開日: 2018-02-13 キーワード (Ja): キーワード (En): 作成者: Oka, Toshihiko, Saiki, Takahiro, Alam, Jahangir Md., Yamazaki, Masahito メールアドレス: 所属:
URL	http://hdl.handle.net/10297/00024649

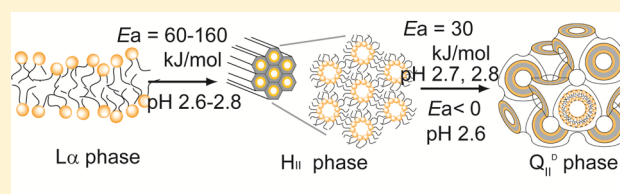
Activation Energy of the Low-pH-Induced Lamellar to Bicontinuous Cubic Phase Transition in Dioleoylphosphatidylserine/Monoolein

Toshihiko Oka,^{†,‡} Takahiro Saiki,[‡] Jahangir Md. Alam,[†] and Masahito Yamazaki^{*,†,‡,§}

[†]Nanomaterials Research Division, Research Institute of Electronics, [‡]Dept. Physics, Graduate School of Science, [§]Integrated Bioscience Section, Graduate School of Science and Technology, Shizuoka University, Shizuoka 422-8529, Japan

Supporting Information

ABSTRACT: Electrostatic interaction is an important factor for phase transitions between lamellar liquid-crystalline (L_{α}) and inverse bicontinuous cubic (Q_{II}) phases. We investigated the effect of temperature on the low-pH-induced L_{α} to double-diamond cubic (Q_{II}^D) phase transition in dioleoylphosphatidylserine (DOPS)/monoolein (MO) using time-resolved small-angle X-ray scattering with a stopped-flow apparatus. Under all conditions of temperature and pH, the L_{α} phase was directly transformed into an intermediate inverse hexagonal (H_{II}) phase, and subsequently the H_{II} phase slowly converted to the Q_{II}^D phase. We obtained the rate constants of the initial step (i.e., the L_{α} to H_{II} phase transition) and of the second step (i.e., the H_{II} to Q_{II}^D phase transition) using the non-negative matrix factorization method. The rate constant of the initial step increased with temperature. By analyzing this result, we obtained the values of its apparent activation energy, E_a ($L_{\alpha} \rightarrow H_{II}$), which did not change with temperature but increased with an increase in pH. In contrast, the rate constant of the second step decreased with temperature at pH 2.6, although it increased with temperature at pH 2.7 and 2.8. These results indicate that the value of E_a ($H_{II} \rightarrow Q_{II}^D$) at pH 2.6 increased with temperature, but the values of E_a ($H_{II} \rightarrow Q_{II}^D$) at pH 2.7 and 2.8 were constant with temperature. The values of E_a ($H_{II} \rightarrow Q_{II}^D$) were smaller than those of E_a ($L_{\alpha} \rightarrow H_{II}$) at the same pH. We analyzed these results using a modified quantitative theory on the activation energy of phase transitions of lipid membranes proposed initially by Squires et al. (Squires, A. M.; Conn, C. E.; Seddon, J. M.; Templar, R. H. *Soft Matter* **2009**, *5*, 4773). On the basis of these results, we discuss the mechanism of this phase transition.



1. INTRODUCTION

Most biomembranes/lipid membranes adopt a lamellar liquid-crystalline (L_{α}) phase, but under certain conditions they form inverse bicontinuous cubic (Q_{II}) phases (e.g., the double-diamond Q_{II}^D (or Q^{224}), the primitive Q_{II}^P (or Q^{229}), and the gyroid Q_{II}^G (or Q^{230}) phases), where the membranes are connected in 3D space with cubic symmetry.^{1–5} In the Q_{II} phase, an infinite periodic minimal surface (IPMS) lies at the bilayer midplane, which is the interface of two monolayers, and the structures of the Q_{II} phases consist of two interwoven networks of water channels, separated by the bilayers.¹ Recently it has been well established that electrostatic interactions due to surface charges of lipid membranes (EI) play various important roles in the structures and phase stabilities of the Q_{II} phase. The electrostatic interactions greatly increases the lattice constants and the size of the water channels of the Q_{II} phase.^{6–10} This may be useful for the crystallization of proteins and the application of biosensors. The modulation of EI induces transitions between the L_{α} and the Q_{II} phases and phase transitions between different Q_{II} phases in various lipids.^{6,7,11–27} Among these phase transitions, pH-induced phase transitions between the Q_{II} phases and the inverse hexagonal (H_{II}) phase^{6,17,21,27} and those between the L_{α} phase and the Q_{II}^D phase¹⁷ have attracted wide attention because the pH is known to control the function and structure of membranes and

proteins, thus playing an indispensable role in cells. We found that the low-pH-induced an L_{α} to Q_{II}^D phase transition in dioleoylphosphatidylserine (DOPS)/monoolein (MO) membranes and that this phase transition was reversible.¹⁷ Low pH decreases the surface charge density of the DOPS/MO membranes by protonation of the carboxylic acid of DOPS, and as a result the decrease in the electrostatic interactions induces the L_{α} to Q_{II}^D phase transition. (See ref 17 for the detailed mechanism.) DOPS and MO are essential biological lipids, and hence we consider that this phase transition has an important physiological meaning. Moreover, this phase transition is one of the best systems for investigating the kinetic pathway of the EI-induced L_{α}/Q_{II} phase transitions because H^+ can rapidly enter the MLVs.²⁸

To reveal the mechanism behind the L_{α}/Q_{II} phase transitions, it is important to elucidate the kinetic pathway. In our previous papers, we investigated the low-pH-induced L_{α} to Q_{II}^D phase transition in DOPS/MO using time-resolved small-angle X-ray scattering (TR-SAXS).^{28,29} In the initial step, the L_{α} phase was directly transformed to the H_{II} phase; subsequently, the H_{II} phase slowly converted to the Q_{II}^D phase. We obtained

Received: October 10, 2015

Revised: January 6, 2016

Published: January 14, 2016

the rate constants of the initial step and of the second step. The appearance of this intermediate state (i.e., the metastable H_{II} phase) was unexpected because this sequence ($L_{\alpha} \rightarrow H_{II} \rightarrow Q_{II}^D$) is different from the phase sequence at equilibrium due to the curvature energy (i.e., the phase appears in order of $L_{\alpha} \rightarrow Q_{II}^D \rightarrow H_{II}$).²⁸ In the temperature–water content phase diagram, a Q_{II} phase appears between the L_{α} and the H_{II} phases during temperature increases or during water content decreases.^{1,30–34} We interpreted that this unusual phenomenon occurs as a kinetic trap as a result of the difference in the activation energy; if the activation energy of the rate-determining step in one kinetic pathway (i.e., the L_{α} to Q_{II}^D phase transition) is much greater than that in the other kinetic pathway (i.e., the L_{α} to H_{II} phase transition), then the L_{α} phase first transforms to the H_{II} phase and then converts to the Q_{II}^D phase.^{28,29}

Generally, the activation energy of structural changes can provide us valuable information on their elementary processes and mechanisms. In this study, to get information on the activation energies of two elementary steps of the low-pH-induced L_{α} to Q_{II}^D phase transition in 20%-DOPS/80%-MO, we investigated the temperature dependence of this phase transition using TR-SAXS. Using a stopped-flow apparatus, a suspension of multilamellar vesicles (MLVs) of 20%-DOPS/80%-MO membrane at neutral pH was rapidly mixed with a low-pH buffer at various temperatures, and then the structural change of the membranes in the resultant suspension was observed as a function of time (i.e., pH-jump experiment). By analyzing these results, the rate constants of two elementary steps (i.e., the initial step (the L_{α} to H_{II} phase transition) and the second step (the H_{II} to Q_{II}^D phase transition)) were obtained at various temperatures. On the basis of these data, we succeeded in obtaining the values and the information on the activation energies of two elementary steps. To our knowledge, these are the first values of the activation energies of the L_{α} to H_{II} phase transition and the H_{II} to Q_{II}^D phase transition of lipid membranes. We analyzed these results using quantitative theory on the activation energy of phase transitions of lipid membranes proposed by Squires et al.³⁵ On the basis of these results, we discuss the mechanism of this phase transition.

2. MATERIALS AND METHODS

MO was purchased from Sigma Chemical Co. (St. Louis, MO, USA). DOPS was purchased from Avanti Polar Lipids (Alabaster, AL, USA). To prepare DOPS/MO-MLVs, 100 μ L of 10 mM ammonium acetate buffer (pH 6.7) containing 100 mM NaCl (buffer A) was added to the dry DOPS/MO lipid film (10 μ mol),²⁸ and then the suspension was mixed several times using a vortex mixer for about 20 s at room temperature (~ 25 °C). To purify the MLVs, the MLV suspension was centrifuged at 13 000g for 20 min at 25 °C, and then the pellet was resuspended gently in new buffer A without using the vortex mixer.²⁸ We used this suspension as the purified MLV suspension. The purified MLVs were used within 12 h after preparation. The lipid concentrations of the suspensions were determined by the Bartlett method.³⁶

Data of temperature scanning SAXS were obtained at the BL-6A beamline of the Photon Factory in KEK (Tsukuba, Japan). The X-ray wavelength was 0.1500 nm, and the sample–detector distance was 1023 mm. Data were collected using a 2D pixel array detector (PILATUS3 1M, Dectris, Baden, Switzerland). A handmade capillary holder with a Peltier device (9504/125/060B, Ferrotec Co., Tokyo, Japan) was used to obtain temperature scan data. The temperature of the holder was controlled with a Peltier controller (TDC-5000A, Cell System Co., Yokohama, Japan) and was measured with a platinum resistance temperature sensor (Pt100), which was connected to the

Peltier controller. Immediately after the purified DOPS/MO-MLV suspension in buffer A was mixed with 20 mM citrate buffer at various pH values containing 100 mM NaCl (buffer C) in a volume ratio of 1:9 in an Eppendorf tube, the resultant suspension was transferred to a quartz capillary tube with a diameter of 1.0 mm and a thickness of 0.01 mm (Hilgenberg GmbH, Malsfeld, Germany), and the ends of the tubes were sealed with silicone grease. This sample in the capillary was incubated for more than 5 h at room temperature (~ 20 °C) before the SAXS measurement. After 10 min of incubation of the sample in the capillary in the holder at 20 °C, the temperature of the sample was increased from 20 to 50 °C at a rate of 1 or 0.5 °C/min. During the temperature scan, the SAXS patterns were measured with a time-resolution of 5 s. Lattice constants were determined by fitting two Gauss functions to the (110) and (111) peaks of the Q_{II}^D phase and one to the (10) peak of the H_{II} phase. Peaks at higher angles were excluded from the fitting because their peak intensities were low. The positions of the peaks at higher angles were used in the phase determination of the samples.

We used the same method of TR-SAXS in our previous paper²⁸ to monitor structural changes in DOPS/MO membranes after a pH jump. TR-SAXS data were obtained at the BL40B2 beamline at SPring-8 (Sayo, Japan). The X-ray wavelength used was 0.1000 nm, and the sample–detector distance was 1150 mm. Data were collected using a 2D pixel array detector (PILATUS 100 K, Dectris, Baden, Switzerland). A stopped-flow apparatus (SFM-CD10, Unisoku, Osaka, Japan) was used to mix rapidly the purified DOPS/MO-MLV suspension in buffer A with 20 mM citrate buffer at various pH values containing 100 mM NaCl (buffer C) in a volume ratio of 1:9. We arranged the stopped-flow apparatus transversely, and thereby the capillary cell was positioned horizontally. The temperature of the apparatus was kept at various values with a water bath circulator (RTE111, Thermo Neslab, NH, USA). After the incubation of the samples (i.e., the MLV suspension and the low-pH buffer) in the stopped-flow apparatus at a specific temperature for 15 min, TR-SAXS measurements were started after 50 ms from a start signal of the stopped-flow apparatus. The mixing dead time of the stopped-flow apparatus was less than 10 ms. The SAXS patterns were recorded for the first 90 s with a resolution of 0.2 s and then for 9 s at various intervals to be equal intervals on a logarithmic time scale of up to 3629 s from the mixing time. The stopped-flow apparatus was moved during X-ray exposure to avoid damage to the sample caused by the X-ray irradiation. After one TR-SAXS measurement of a sample at low pH, we washed the capillary in the stopped-flow apparatus by running the same buffer, distilled water, ethanol, and distilled water several times, and then we measured the SAXS pattern of the capillary containing a buffer to confirm that no membranes were adsorbed in the capillary cell.

The lattice constant, a , of the Q_{II}^D phase is determined by $S = (1/a)\sqrt{h^2 + k^2 + l^2}$, and that of the H_{II} phase, which equals the center-to-center distance of adjacent cylinders in the H_{II} phase, is determined by $S = (2/\sqrt{3}a)\sqrt{h^2 + k^2 + hk}$, where S is the reciprocal spacing and h , k , and l are Miller indices. A series of sequential 2D ring diffraction patterns were averaged circularly to reduce them to a set of sequential 1D patterns. These patterns were corrected by subtracting the background scatter caused by the capillary and the buffer. The sequential 1D diffraction patterns are equivalent to matrix $X(S, t)$ in which matrix element X_{ij} corresponds to the intensity at the i th scattering vector S_i and j th delay time t_j . $m \times n$ matrix X is the product of the $m \times k$ matrix of the pure component diffraction profiles A and the $n \times k$ matrix of the concentration time courses B , where k is the number of components

$$X = AB^T + E$$

where superscript T denotes the transpose of the matrix. E is the residual matrix containing the data variance or statistical noise which is not explained by AB^T . To analyze matrix X , we applied a non-negative matrix factorization (NMF) method based on a modified alternating least-squares (MALS) algorithm.^{37,38} In a typical MALS algorithm, optimized values of A and B are calculated from a random matrix

alternatingly with the constraint that the values in A and B are non-negative. Given fluctuations in the data, we adopted two constraints as follows: (1) the mean values of the adjacent points are non-negative for matrix A or larger than -1σ for matrix B ; (2) the mean value of the first points in matrix B without a first component is within $\pm 1\sigma$. Parameter σ is the standard deviation of data in the corresponding region. The program was coded on GNU Octave. We used a k value of 3, which is the number of components we could distinguish from the contour maps. Data up to 3629 s were used in the calculations. We repeated independent MALS calculations more than 10 times. Converged matrices A from the independent calculations were almost identical; this was also true for the B matrices.

3. RESULTS

3.1. Temperature–pH Phase Diagram of 20%-DOPS/80%-MO. First we investigated the temperature-induced phase transitions of 20%-DOPS/80%-MO (molar ratio) membranes at various pH values from pH 2.6 to 2.8. The contour plot shows the SAXS patterns of 20%-DOPS/80%-MO membranes at pH 2.7 recorded during a temperature scan from 20 to 50 °C at a rate of 1 °C/min (Figure 1a). A waterfall plot of the same data is shown in Figure S1 in Supporting Information (SI). At 20 °C, the SAXS peaks which have a spacing ratio of $\sqrt{2}:\sqrt{3}:\sqrt{4}:\sqrt{6}:\sqrt{8}:\sqrt{9}$ were indexed as the (110), (111), (200), (211), (220), and (221) peaks of a Q_{II}^D phase (Figure 1b).⁶ At 35 °C, a new weak peak appeared at around $S = 0.170 \text{ nm}^{-1}$, and its intensity increased with time. The SAXS pattern at 50 °C shows the SAXS peaks which have a spacing ratio of $1:\sqrt{3}:2$, corresponding to the H_{II} phase, indicating that the peak at $S = 0.179 \text{ nm}^{-1}$ was due to the (10) peak of the H_{II} phase. Thereby this result indicates that a Q_{II}^D to H_{II} phase transition started to occur at 35 °C. At 50 °C, the peak intensity of the H_{II} phase became strong, but weak, broad peaks probably due to the distorted Q_{II}^D remained around $S = 0.13\text{--}0.15 \text{ nm}^{-1}$. At final pH 2.6, we obtained a similar result (Figure S2). Although the peak positions of the (200) peak of the Q_{II}^D phase and the (10) peak of the H_{II} phase were similar, on the basis of the other peaks of the H_{II} phase and the intensity of the (110) and (111) peaks of the Q_{II}^D phase, we can judge that a Q_{II}^D to H_{II} phase transition started to occur at 35 °C.

Figure 1c shows the temperature dependence of the lattice constants of the H_{II} and Q_{II}^D phases. The lattice constant of the Q_{II}^D phase was almost constant at lower temperature, but at above 31 °C it decreased with temperature. On the other hand, the lattice constant of the H_{II} phase decreased from 6.8 nm with an increase in temperature. This result agrees with the temperature dependence of the lattice constant of the H_{II} phase in other lipid membranes.^{32,39} We obtained similar results for the temperature scan from 20 to 50 °C at a rate of 0.5 °C/min.

On the basis of these SAXS experiments, we made the temperature–pH phase diagram (Figure 1d) after the correction of the pH of the solution using data on the temperature dependence of the pH value (Figure S3). The phase transition from the Q_{II}^D to the H_{II} phase occurred as temperature increased, which agrees with other researches.^{31,39} The transition temperature from the Q_{II}^D to the H_{II} phase, $T_{Q \rightarrow H}$ increased a little with an increase in pH.

3.2. Kinetics of the Low-pH-Induced L_α to Q_{II}^D Phase Transition of 20%-DOPS/80%-MO at Various Temperatures. As described in our previous paper,²⁷ 20%-DOPS/80%-MO membranes at neutral pH are in the L_α phase (Figure S4(a)). First we conducted TR-SAXS experiments at a final pH of 2.6 at 20 °C. After the purified MLV suspension in buffer A was rapidly mixed with buffer C (pH 2.4) at 20 °C, the

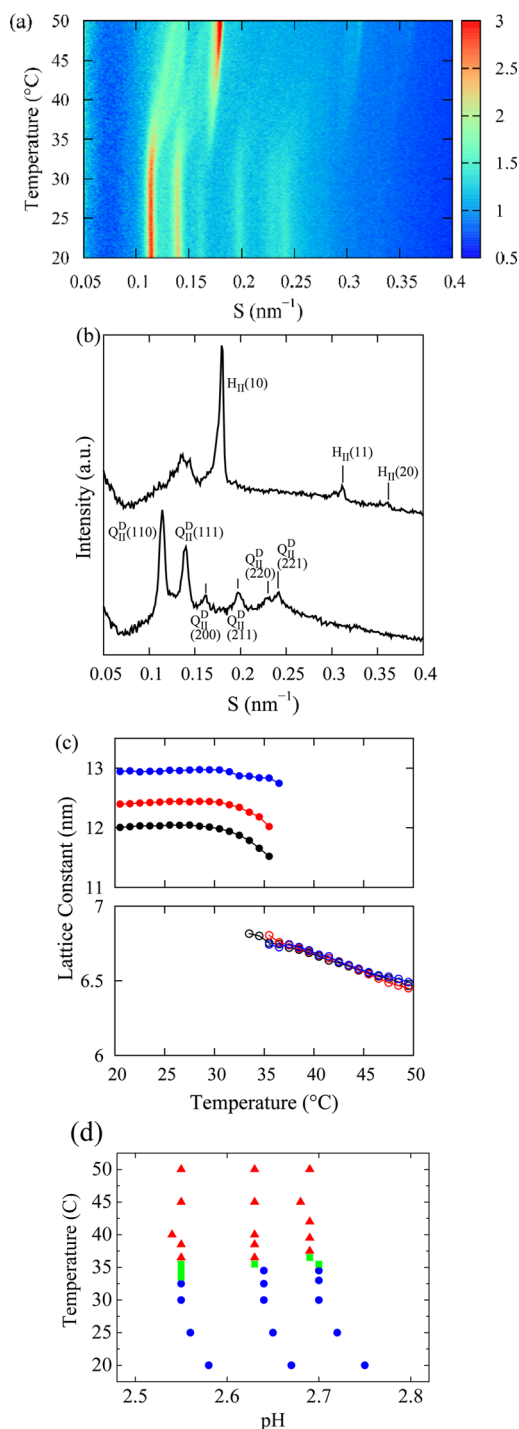


Figure 1. Changes in structure and phase of 20%-DOPS/80%-MO membranes at low pH during a temperature scan from 20 to 50 °C at a rate of 1 °C/min (8.3 mM lipid concentration). (a) SAXS contour plot of the temperature scan at pH 2.7. (b) Averaged SAXS patterns of the data shown in (a) from 20.0 to 21.0 °C (bottom) and from 49.0 to 50.0 °C (top). (c) Temperature dependence of the lattice constants of the Q_{II}^D (in the upper figure) and of the H_{II} phases (in the lower figure). (black ●, ○) pH 2.6, (red ●, ○) pH 2.7, and (blue ●, ○) pH 2.8. (d) Temperature–pH phase diagram. (blue ●) the Q_{II}^D phase, (green ■) coexistence of the Q_{II}^D and H_{II} phases, and (red ▲) coexistence of the H_{II} phase and unidentified structure.

structure and the phase of the membranes in the resultant suspension (final pH 2.6) changed with time. The contour plot shows the time course of the SAXS patterns of this sample

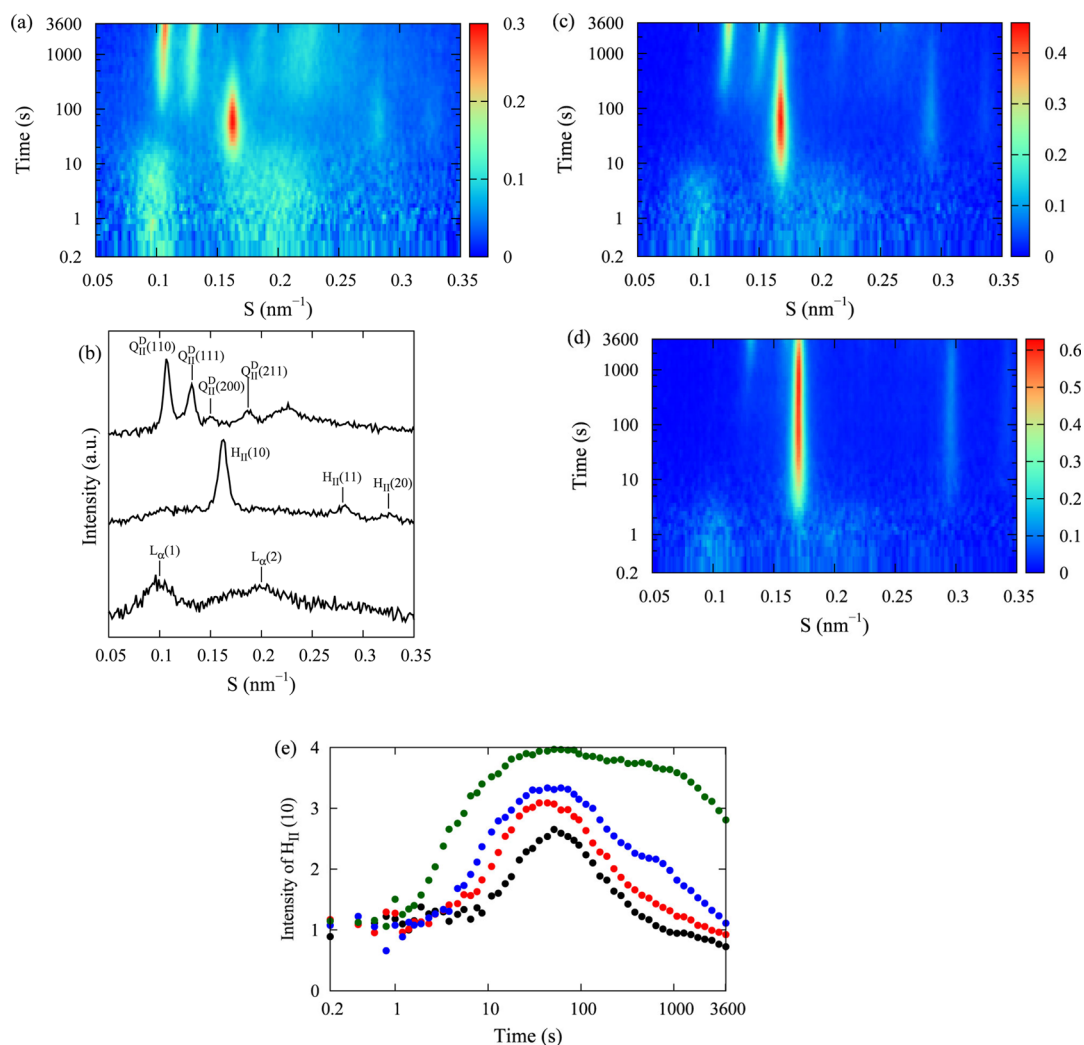


Figure 2. Changes in structure and phase of 20%-DOPS/80%-MO membranes after the pH jump from pH 6.7 to pH 2.6 at various temperatures (7.5 mM lipid concentration). (a) SAXS contour plot of the time course at 20 °C (a), 30 °C (c), and 35 °C (d). (b) Averaged SAXS patterns of the data shown in (a) from 0.2 to 2 s (bottom), from 50 to 59 s (middle), and from 3620 to 3629 s (top). (e) Integrated intensity of the (10) peak of the H_{II} phase; at 20 °C (black), at 25 °C (red), at 30 °C (blue), and at 35 °C (green).

(Figure 2a), and the waterfall plot of the same data is shown in Figure S5. From 0 to 10 s, only SAXS peaks corresponding to the L_{α} phase were observed (Figure 2a,b). At 10 s after mixing, a new weak peak appeared at around $S = 0.163 \text{ nm}^{-1}$, and its intensity increased with time. The SAXS pattern at 50 s (Figure 2a,b) shows peaks which have a spacing ratio of $1:\sqrt{3}:2$, corresponding to an H_{II} phase, indicating that the peak at $S = 0.163 \text{ nm}^{-1}$ was due to the (10) peak of the H_{II} phase. The intensities of the peaks of the H_{II} phase increased with time up to 50 s and then decreased (Figure 2e, black curve), whereas those of the L_{α} phase became low at 50 s. At 100 s, two weak peaks at $S = 0.107$ and 0.131 nm^{-1} appeared, and their intensities increased with time. We also measured the SAXS pattern of the same sample following a long incubation (10 h at 25 °C) (Figure S4(b)); this pattern should correspond to the equilibrium structure. Peaks which have a spacing ratio of $\sqrt{2}:\sqrt{3}:\sqrt{4}:\sqrt{6}:\sqrt{8}:\sqrt{9}$ were indexed as the (110), (111), (200), (211), (220), and (221) peaks of a Q_{II}^D phase; its lattice constant was 11.5 nm. On the basis of the equilibrium structure, the peaks at $S = 0.107$ and 0.131 nm^{-1} in Figure 2a were assigned as the (110) and (111) peak of the Q_{II}^D phase, respectively.

The result of the same experiment at 30 °C (Figure 2c) shows that the peak of the H_{II} phase appeared earlier but the peaks of the Q_{II}^D phase appeared later compared to those at 20 °C (Figure 2a). In contrast, at 35 °C (Figure 2d), the (10) peak of the H_{II} phase started to appear at 3 s, but the (110) and (111) peaks of the Q_{II}^D phase started to appear at ~ 1000 s. Figure 2e shows the time course of the intensity of the (10) peak of the H_{II} phase at various temperatures, indicating that with an increase in temperature the H_{II} phase started to appear earlier. Especially at 35 °C, we observed only small peaks of the Q_{II}^D phase 1 h after mixing, indicating that the rate of the transition from the H_{II} to the Q_{II}^D phase was very slow (i.e., the membranes were almost trapped in the intermediate H_{II} phase). The lattice constant of the H_{II} phase decreased with temperature from 7.1 nm (at 20 °C) to 6.8 nm (35 °C) (Table 1).

We conducted the same TR-SAXS experiments at final pH values of 2.7 and 2.8 at various temperatures and obtained similar results. (See the quantitative analysis in the Discussion section.)

Table 1. Temperature Dependence of the Lattice Constants at Various pH Values^a

temperature (°C)	L_α (initial) (nm)	H_{II} (intermediate) (nm)	Q_{II}^D (1 h) (nm)
(a) Final pH 2.6			
20	10	7.1	13.2
25	10	7.0	12.1
30	10	6.9	11.3
35	10	6.8	10.8
(b) Final pH 2.7			
20	10	7.2	14.1
25	10	7.0	12.9
30	10	7.0	11.9
35	10	6.8	11.2
(c) Final pH 2.8			
20	10		
25	10	7.1	13.7
30	10	7.0	12.5
35	10	6.9	11.8

^aLattice constants for the Q_{II}^D phase 1 h after mixing with the low-pH buffer were determined.

4. DISCUSSION

The results of the temperature scan of the SAXS measurements clearly show that for the 20%-DOPS/80%-MO membranes at low pH (2.6–2.8) the Q_{II}^D to H_{II} phase transition started to occur at 33–35 °C (depending on pH). This result agrees with the results of other cubic systems of lipid membranes.^{31,34,39} In excess water, the membrane in the H_{II} phase has a large negative curvature close to the spontaneous curvature,^{40,41} and thereby the radius of the water cylinder in the H_{II} phase which is defined as the distance between the center of the water cylinder and the neutral surface of the monolayer, R_w , is almost the same as the radius of the spontaneous curvature, R_0 . It is reported that the $|H_0|$ of phosphatidylethanolamine (PE) monolayers increases with temperature.^{34,40,41} As shown in Figure 1c, the lattice constant a of the H_{II} phase of 20%-DOPS/80%-MO decreased with temperature. In other lipid systems, a of the H_{II} phase decreased with temperature.⁴¹ Since $a = 2(R_w + d_m)$ where d_m is the thickness of the monolayer and the temperature dependence of d_m is very small, $\Delta a \approx 2\Delta R_w$.⁴¹ Thereby, the decrease in a with temperature indicates that R_w decreases with temperature; therefore, $|H_0|$ of this monolayer increases with temperature (i.e., H_0 decreases with temperature). The free energy of the L_α phase (G_{L_α}) of this membrane is large due to the curvature elastic energy, $G_{L_\alpha}^{curv} (= \kappa H_0^2 A/2$, where κ is the bending modulus of monolayer and A is the area of membranes), since the mean curvature of the membrane in the L_α phase is 0; therefore, G_{L_α} increases with temperature. In contrast, the free energy of the H_{II} phase ($G_{H_{II}}$) due to the curvature elastic energy is very small, but $G_{H_{II}}$ is large due to the interstitial chain packing energy of the H_{II} phase, $G_{H_{II}}^{pack}$.^{29,41,42} Hence, the difference between the free energy of the H_{II} phase and that of the L_α phase, $\Delta G_{H-L} (= G_{H_{II}} - G_{L_\alpha})$ can be described as follows.

$$\Delta G_{H-L} = G_{H_{II}} - G_{L_\alpha} = G_{H_{II}}^{pack} - \kappa H_0^2 A/2 \quad (1)$$

Therefore, ΔG_{H-L} decreases with an increase in $|H_0|^2$, and $\Delta G_{H-L} = 0$ at the transition temperature from the L_α to the H_{II} phases, $T_{L \rightarrow H}$.^{29,40,41} On the other hand, the difference between

the free energy of the Q_{II}^D phase ($G_{Q_{II}^D}$) and G_{L_α} , $\Delta G_{Q-L} (= G_{Q_{II}^D} - G_{L_\alpha})$, can be described as follows.^{34,43,44}

$$\Delta G_{Q-L} = G_{Q_{II}^D} - G_{L_\alpha} = \bar{\kappa}_{bil} \langle K \rangle A$$

$$\text{where } \bar{\kappa}_{bil} = 2(\bar{\kappa}_m - 4\kappa H_0 \xi) \quad (2)$$

where $\bar{\kappa}_{bil}$ is the Gaussian curvature modulus of the bilayer, $\langle K \rangle$ is the average value of the Gaussian curvature of the membrane over its total neutral surface area A , $\bar{\kappa}_m$ is the Gaussian curvature modulus of the monolayer, and ξ is the distance between the bilayer midplane and monolayer's neutral surface. Therefore, ΔG_{Q-L} decreases with an increase in $|H_0|$, and $\Delta G_{Q-L} = 0$ at the transition temperature from the L_α to the Q_{II}^D phases, $T_{L \rightarrow Q}$.^{3,29,34} If $T_{L \rightarrow Q}$ is less than $T_{L \rightarrow H}$, then as the temperature increases, phase transitions occur according to the phase sequence of $L_\alpha \rightarrow Q_{II}^D \rightarrow H_{II}$, and the Q_{II}^D to H_{II} phase transition occurs at $T_{Q \rightarrow H}$ when $G_{H_{II}} = G_{Q_{II}^D}$.⁴⁵

The lattice constant of the H_{II} phase (6.8 nm) which was observed initially after the Q_{II}^D to H_{II} phase transition during the temperature scan (i.e., at ~35 °C) (Figure 1c) is almost the same as that of the intermediate state of the low-pH-induced L_α to Q_{II}^D phase transition of the 20%-DOPS/80%-MO membrane at 35 °C (6.8 nm, Table 1). This supports that the identification of the intermediate state as the H_{II} phase is valid.

The results of Figure 1 show that the lattice constant of the Q_{II}^D phase was almost constant from 20 to 31 °C at a heating rate of 0.5–1.0 °C/min but above 31 °C (before starting the transition) it decreased greatly with temperature. Recently, Barriga et al. reported that the binary mixture of MO with a small amount of DOPS or dioleoylphosphatidylglycerol (DOPG) in water under nonexcess water conditions (70 wt % water) shows an increase in the lattice constant with an increase in temperature.⁴⁶ This is an interesting difference, but currently we do not know its reason.

The results of TR-SAXS measurements clearly show the temperature dependence of the kinetic pathway of the low-pH-induced L_α to Q_{II}^D phase transition of the 20%-DOPS/80%-MO membrane. Here, we analyze the kinetics of this phase transition quantitatively using the same method described in our previous paper.²⁸ In the low-pH-induced L_α to Q_{II}^D phase transition of the purified MLVs (e.g., Figure 2a), SAXS peaks due to each phase were well separated. We therefore applied the NMF method^{37,38} to obtain the rate constant of each step of the phase transition. The results of the NMF method are shown in Figure 3. Figure 3a–c indicates three components in the data (i.e., the L_α (a), the H_{II} (b), and the Q_{II}^D phases (c)). Figure 3d–f indicates the time course of each component. We can divide the time course into two stages. In the first stage up to around 50 s, the amount of the L_α phase decreased, the H_{II} phases increased, and the Q_{II}^D phase remained almost 0. Most of the membranes in the L_α phase, therefore, were converted to the H_{II} phase. In the second stage from 50 to 3629 s, the amount of the H_{II} phase decreased but that of the Q_{II}^D phase increased. Therefore, in the second stage, the phase transition occurred from the H_{II} to the Q_{II}^D phase. To fit the data of the decrease in intensity of the H_{II} phase (Figure 3e), two rate constants were required for the H_{II} to Q_{II}^D phase transition; one is for the fast transition from the H_{II} to the Q_{II}^D phase (k_{2F}), and the other is for the slow transition from the H_{II} to the Q_{II}^D phase (k_{2S}). The basic scheme of the phase transitions is as follows.

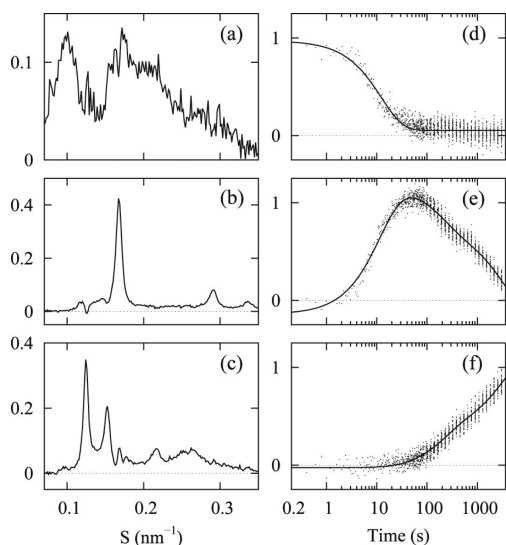
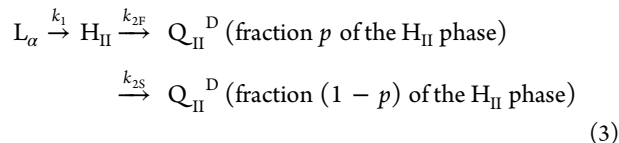


Figure 3. Results from the MALS calculations of the SAXS pattern of a 20%-DOPS/80%-MO membrane suspension from 0.2 to 3629 s after the pH jump from 6.7 to 2.6 at 30 °C (Figure 2c). Restored SAXS profiles of matrix A corresponding to the L_α , H_{II} , and Q_{II}^D phases are shown in a–c, respectively. The time courses of the SAXS intensities of matrix B corresponding to the L_α , H_{II} , and Q_{II}^D phases are shown in d–f, respectively.



where k_1 is the rate constant of the transition from the L_α to the H_{II} phase. The time courses of the concentration of each phase are described using the following differential equations.

$$\frac{d[L_\alpha]}{dt} = -k_1[L_\alpha]$$

$$\frac{d[H_{II}]}{dt} = k_1[L_\alpha] - \{pk_{2F} + (1 - p)k_{2S}\}[H_{II}]$$

$$\frac{d[Q_{II}^D]}{dt} = \{pk_{2F} + (1 - p)k_{2S}\}[H_{II}]$$
(4)

The solutions for these differential equations under the initial condition ($[L_\alpha] = C_0$ at $t = 0$) are as follows.

$$[L_\alpha] = C_0 \exp(-k_1 t)$$

$$[H_{II}] = \frac{k_1 C_0}{\{pk_{2F} + (1 - p)k_{2S}\} - k_1} [\exp(-k_1 t) - \exp[-\{pk_{2F} + (1 - p)k_{2S}\}t]]$$

$$[Q_{II}^D] = \frac{k_1 C_0 \{pk_{2F} + (1 - p)k_{2S}\}}{\{pk_{2F} + (1 - p)k_{2S}\} - k_1} \{k_1 \exp[-\{pk_{2F} + (1 - p)k_{2S}\}t] - \{pk_{2F} + (1 - p)k_{2S}\} \exp(-k_1 t) + k_1 C_0 \{pk_{2F} + (1 - p)k_{2S}\}\}$$
(5)

The time courses in Figure 3 are not the fractions of components, and the values might not start from or end at 0. We modified the equations as follows.

$$[L_\alpha] = A_0 \exp(-k_1 t) + B_0$$

$$[H_{II}] = A_1 \{\exp(-k_1 t) - \exp[-\{pk_{2F} + (1 - p)k_{2S}\}t]\} + B_1$$

$$[Q_{II}^D] = A_2 \{k_1 \exp[-\{pk_{2F} + (1 - p)k_{2S}\}t] - \{pk_{2F} + (1 - p)k_{2S}\} \exp(-k_1 t)\} + B_2$$
(6)

The time course of the SAXS intensities of the three phases for the data of Figure 2c (final pH 2.6 at 30 °C) was fit well by eq 6 (Figure 3d–f), providing $k_1 = 0.081 \text{ s}^{-1}$, $k_{2F} = 0.0050 \text{ s}^{-1}$, $k_{2S} = 0.00031 \text{ s}^{-1}$, and $p = 0.35$. As shown in Table 2, values of k_1 were 2–17 times larger than those of k_{2F} at same pH and temperature. It is noted that the accuracy of the values of k_{2S} was not high because the measuring time was 3600 s, which is

Table 2. pH Dependence of the Rate Constants

	(a) k_1 (s^{-1}) ^a			
	pH 2.6	pH 2.7	pH 2.8	
20 °C	0.0362 ± 0.0008	0.0175 ± 0.0004	ND	
25 °C	0.072 ± 0.001	0.058 ± 0.001	0.0041 ± 0.0001	
30 °C	0.081 ± 0.001	0.068 ± 0.001	0.019 ± 0.0004	
35 °C	ND	ND	0.033 ± 0.0005	
	(b) k_{2F} , ^b k_{2S} , ^c and p ^d			
	pH 2.6	pH 2.7	pH 2.8	
20 °C	k_{2F} (s^{-1})	0.0055 ± 0.0002	0.0043 ± 0.0006	ND
	k_{2S} (s^{-1})	0.00018 ± 0.00002	0.00072 ± 0.00002	ND
	p	0.71 ± 0.01	0.38 ± 0.03	ND
25 °C	k_{2F} (s^{-1})	0.0043 ± 0.0001	0.0048 ± 0.0002	0.0022 ± 0.0002
	k_{2S} (s^{-1})	0.00024 ± 0.00002	0.00033 ± 0.00002	0.00011 ± 0.00006
	p	0.62 ± 0.01	0.60 ± 0.01	0.87 ± 0.02
30 °C	k_{2F} (s^{-1})	0.0050 ± 0.0002	0.0067 ± 0.0003	0.0024 ± 0.0001
	k_{2S} (s^{-1})	0.00031 ± 0.00001	0.00071 ± 0.00001	0.00016 ± 0.00002
	p	0.35 ± 0.01	0.44 ± 0.01	0.66 ± 0.02
35 °C	k_{2F} (s^{-1})	ND	ND	0.0032 ± 0.0002
	k_{2S} (s^{-1})	ND	ND	0.00028 ± 0.00001
	p	ND	ND	0.35 ± 0.01

^aRate constants of the initial step (i.e., the L_α to H_{II} phase transition). ^bRate constants of the fast transition from the H_{II} to the Q_{II}^D phase. ^cRate constant of the slow transition from the H_{II} to the Q_{II}^D phase. ^dFraction of the H_{II} phase which follows the fast transition.

not sufficient to determine accurate values of k_{2S} . At present, we do not know the origin of the slower component of the H_{II} to the Q_{II}^D phase transition (k_{2S}). The rate constant of the second step may depend on the size of the membranes.

Next we consider the temperature dependence of the rate constants of both steps. The k_1 values greatly increased with temperature for all pH values. Figure 4a shows the graphs of

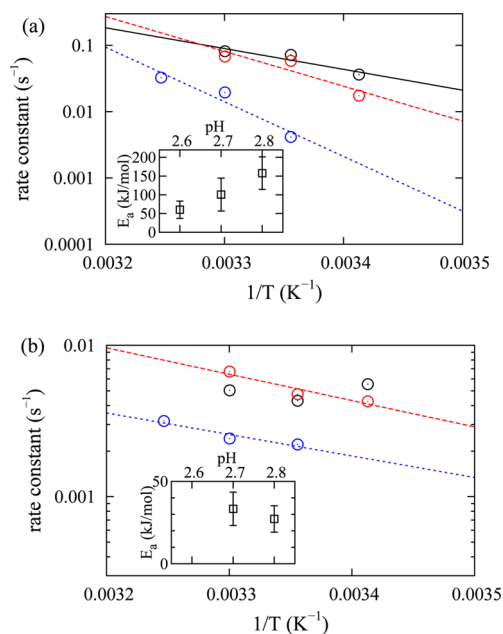


Figure 4. Temperature dependence of the rate constant. (a) $\log_{10} k_1$ vs $1/T$ at final pH 2.6 (black), at pH 2.7 (red), and at pH 2.8 (blue). The inset is the pH dependence of the apparent activation energy, E_a ($L_\alpha \rightarrow H_{II}$). (b) $\log_{10} k_2$ vs $1/T$ at final pH 2.6 (black), at pH 2.7 (red), and at pH 2.8 (blue). The inset is the pH dependence of the apparent activation energy, E_a ($H_{II} \rightarrow Q_{II}^D$).

$\log_{10} k_1$ vs $1/T$ (where T is absolute temperature) at various pH values. Since $k = A \exp(-E_a/RT)$, where E_a is apparent activation energy, R is the gas constant, and A is a constant called the pre-exponential factor, the value of E_a can be determined using an equation of $-2.30R \times$ (slope of the curve of $\log_{10} k$ vs $1/T$). As the temperature increased from 20 to 35 °C, the pH of the suspension changed by less than 0.5 (Figure S3). At all pH values, the data were well fit linearly, indicating that E_a ($L_\alpha \rightarrow H_{II}$) does not depend on temperature (i.e., it is constant). Therefore, we were able to obtain the values of E_a ($L_\alpha \rightarrow H_{II}$) increased with an increase in pH from 60 ± 20 kJ/mol at pH 2.6 to 160 ± 40 kJ/mol at pH 2.8 (Figure 4a inset). The appearance of the intermediate H_{II} phase in the low-pH-induced L_α to Q_{II}^D phase transition can be explained by a greater activation energy of the direct transition from the L_α to Q_{II}^D phase, E_a ($L_\alpha \rightarrow Q_{II}^D$), than E_a ($L_\alpha \rightarrow H_{II}$). As shown in Table 2a, k_1 increased greatly with a decrease in pH at same temperature, which can be explained by the decrease in E_a ($L_\alpha \rightarrow H_{II}$) with a decrease in pH (Figure 4a). Here we did not make a correction to the pH (i.e., the pH in Figure 4 is the pH at 20 °C) but considered it to be an experimental error of the values of E_a . We estimated the corrected values of E_a (i.e., E_a') by using the corrected rate constants of the same pH determined by the linear interpolation of the values of the rate constants at the same $1/T$. These values of E_a' were a little

smaller than those of E_a without correction, but the E_a' values existed within the experimental error of the E_a values in the insets of Figure 4 (details in SI).

In the process of the L_α to H_{II} phase transition, at first the neighboring bilayers in the L_α phase must contact each other at a local site due to their thermal fluctuation (Figure S8a), and then the apposed (cis) monolayers fuse to form stalk structures (or the trans monolayer contact) (Figure S8b).^{47,48} We consider that the stalk structures involve the transition state, which determines E_a ($L_\alpha \rightarrow H_{II}$). The surface charge density of the DOPS/MO membrane increases with an increase in pH because the protonation of the carboxylic acid of DOPS becomes smaller at higher pH. Therefore, we can reasonably consider that the electrostatic interactions inside the membrane in the stalk structure increase with an increase in pH, resulting in the increase in E_a ($L_\alpha \rightarrow H_{II}$).

In contrast, the value of k_{2F} decreased slightly with temperature for pH 2.6, although the k_{2F} values for pH 2.7 and 2.8 slightly increased with temperature (Table 2b). We obtained the values of E_a ($H_{II} \rightarrow Q_{II}^D$) by the slope of the curves at pH 2.7 and 2.8 (Figure 4b). The result at pH 2.6 indicates that E_a ($H_{II} \rightarrow Q_{II}^D$) increases with temperature. On the other hand, E_a ($H_{II} \rightarrow Q_{II}^D$) at pH 2.7 and 2.8 was 30 ± 10 kJ/mol (Figure 4b inset). These values of E_a ($H_{II} \rightarrow Q_{II}^D$) were smaller than those of E_a ($L_\alpha \rightarrow H_{II}$) at the same pH. However, the values of k_1 were greater than those of k_{2F} at same pH (Table 2). Therefore, we conclude that the pre-exponential factor of the rate constant of the second step (i.e., the H_{II} to Q_{II}^D phase transition) is much smaller than that of the first step (i.e., the L_α to H_{II} phase transition). In other words, the frequency of the attempt of the H_{II} to Q_{II}^D phase transition is much smaller than that of the L_α to H_{II} phase transition. As described above, the stalk structures involve the transition state from the L_α to H_{II} phase transition, which determines E_a ($L_\alpha \rightarrow H_{II}$). The thermal fluctuation of bilayer in the L_α phase is so large that the attempt to form local contacts between neighboring membranes occurs frequently and hence the pre-exponential factor of the L_α to the H_{II} phase transition is much greater than that of the H_{II} to Q_{II}^D phase transition.

In the present study, we obtained the values of the apparent activation energy of the elementary steps of the low-pH-induced L_α to Q_{II}^D phase transition in 20%-DOPS/80%-MO. The values of E_a ($L_\alpha \rightarrow H_{II}$) were 60–160 kJ/mol, and those of E_a ($H_{II} \rightarrow Q_{II}^D$) were 30 kJ/mol. To our knowledge, the values of the activation energies of the L_α to H_{II} phase transition and the H_{II} to Q_{II}^D phase transition of lipid membranes have never been published; therefore, it is difficult to compare these values with those of other lipid membranes. During the phase transitions from L_α to H_{II} and from H_{II} to Q_{II}^D , the rupture of the membrane must occur because these phases are topologically different. It is considered that during the L_α to H_{II} (or Q_{II}^D) phase transition after the trans monolayer contact (TMC) or hemifusion intermediate is produced (Figure S8c), there are two patterns of structural changes from the TMC.⁴⁸ If the trans monolayers at the TMC rupture, then an interlamellar attachment (ILA) or a fusion pore (Figure S8e) is formed (type A). If ILAs accumulate in sufficient numbers, they form ILA lattices, which are transient intermediates in Q_{II} phase formation. If rupture does not occur and TMCs accumulate and aggregate, the H_{II} phase appears (Figure S8d) (type B). The rate of bilayer rupture determines the relative rate of H_{II} phase formation.⁴⁸ Recently, the activation energies of the tension (σ)-induced rupture of the bilayer, E_a (rupture), have

been determined; in the case of the electrically neutral dioleoylphosphatidylcholine (DOPC) bilayer, E_a (rupture) = 49 kJ/mol at $\sigma = 7.0$ mN/m and E_a (rupture) decreased with an increase in tension.⁴⁹ It is considered that E_a (rupture) decreases greatly with an increase in the electrostatic interactions due to surface charges of the bilayer.⁵⁰ Since the 20%-DOPS/80%-MO membrane is a charged membrane, we can expect that E_a (rupture) is smaller but increases with a decrease in pH. Therefore, we can consider that E_a ($L_\alpha \rightarrow H_{II}$) is larger than E_a (rupture) but E_a ($H_{II} \rightarrow Q_{II}^D$) is similar to E_a (rupture).

The rate constant of the initial step, k_1 , increased with temperature. By analyzing this result using the standard method, we obtained the values of E_a ($L_\alpha \rightarrow H_{II}$), which did not change with temperature. As described above, the free energy of the L_α phase (G_{L_α}) of this membrane increases with temperature due to the increase in $|H_0|$. Therefore, we can infer that the free energy of the transition state from the L_α phase to the H_{II} phase, G^\ddagger ($L_\alpha \rightarrow H_{II}$), increases with temperature so that E_a ($L_\alpha \rightarrow H_{II}$) becomes constant with temperature. However, when we consider the phase transitions or the reactions whose transition state's free energy depends on temperature, we need a suitable theory for its activation energy. Squires et al. proposed a quantitative theory of the activation energy $\Delta G^\ddagger(T)$ of phase transitions of lipid membranes from phase A to phase B involving changes in monolayer curvature.³⁵ This theory can reasonably explain the pressure (P)-induced phase transition between Q_{II}^D and Q_{II}^P . They assumed that the activation energy is determined only by the change in the curvature elastic energy and thereby obtained the following equation.

$$\Delta G^\ddagger(T) = G^\ddagger - G_A = \Delta G^{\ddagger'} + N_A N_{\text{coop}} A_n \{(g^\ddagger(T) - g^{\ddagger'}) - (g_A(T) - g_A')\} \quad (7)$$

where G^\ddagger is the free energy of the transition state; $\Delta G^{\ddagger'}$ is the activation energy at the phase boundary between phases A and B, where the free energy of both phases are the same, $G_A = G_B$; N_A is Avogadro's number; N_{coop} is the number of molecules in a cooperative unit; A_n is the cross-sectional area per molecule at the pivotal surface; $g^\ddagger(T)$ and $g^{\ddagger'}$ are the curvature elastic energy per unit area of the transition state at T and at the phase boundary, respectively; and $g_A(T)$ and g_A' are the curvature elastic energy per unit area of phase A at T and at the phase boundary, respectively. For the equation of g , the Helfrich's expression⁵¹ is used as follows.

$$g = 2\kappa(H - H_0)^2 + \bar{\kappa}_m K$$

If we assume that Gaussian curvature K and κ are constants (i.e., not depend on temperature), then eq 7 is converted to the following equation³⁵

$$\Delta G^\ddagger(T) = G^\ddagger - G_A = \Delta G^{\ddagger'} + 2\kappa N_A N_{\text{coop}} A_n \{(H^\ddagger - H_0)^2 - (H^{\ddagger'} - H_0')^2 - (H_A - H_0)^2 + (H_A' - H_0')^2\} \quad (8)$$

where H^\ddagger and H_A are the mean curvature of the transition state and phase A, respectively, and ' denotes the physical quantity at the phase boundary. Squires et al. assumed that H^\ddagger and H_A are constants (i.e., not depend on temperature) because their membrane systems were under limited hydration conditions.³⁵

In this case, eq 8 can be converted to the following equation, which is the main equation in the theory of Squires et al.³⁵

$$\Delta G^\ddagger = \Delta G^{\ddagger'} - 4\kappa N_A N_{\text{coop}} A_n (H_0 - H_0')(H^\ddagger - H_A) \quad (9)$$

However, in our case we investigated DOPS/MO membranes in excess water, and hence it is difficult to adopt the assumption of Squires et al. The result of Figure 1c clearly shows that the mean curvature of the H_{II} phase, $H_{H_{II}}$, decreases with an increase in temperature, which supports our consideration. Therefore, we consider here that H^\ddagger and H_A depend on temperature, and as a result we use eq 8 instead of eq 9.

First we consider the initial step of the low-pH-induced L_α to Q_{II}^D phase transition in 20%-DOPS/80%-MO (i.e., the L_α to H_{II} phase transition). In this case, phase A is the L_α phase and phase B is the H_{II} phase, and both the phases are stable or metastable states, which have a free-energy minimum. We consider that another stable state does not exist during the L_α to H_{II} phase transition. However, as we described above, during the L_α to H_{II} phase transition there are many transient, unstable states such as membranes containing the stalk, the TMC, and the close contact at local sites (Figure S6), and the most unstable state which has the highest free energy is called the transition state. As defined in eq 7, the activation energy from the L_α to H_{II} phase transition is defined as the difference between the free energy of the transition state and that of the L_α phase; therefore, the activation energy does not depend on many unstable states during the reaction path from the L_α to the H_{II} phase. Since phase A is the L_α phase, $H_A = H_{L_\alpha} = 0$. We assume that the mean curvature of the transition state H^\ddagger of the L_α to H_{II} phase transition can be expressed by the first-order approximation of temperature in the small temperature range, and hence H^\ddagger ($L_\alpha \rightarrow H_{II}$) = $C_1 + \beta T$, where C_1 and β are constants. On the other hand, it is well known that H_0 of lipid membranes decreases linearly with temperature.^{35,44,52,53} Here we also assume that H_0 of the 20%-DOPS/80%-MO monolayer decreases linearly with temperature (i.e., $H_0 = -C_0 - \alpha T$, where C_0 and α are positive constants). Therefore, $H_0 - H_0' = -\alpha \Delta T$, where $\Delta T = T - T'$ and T' is the temperature at the phase boundary or the phase-transition temperature. Using eq 8, we can obtain the activation energy of this phase transition, ΔG^\ddagger ($L_\alpha \rightarrow H_{II}$), as follows.

$$\Delta G^\ddagger(L_\alpha \rightarrow H_{II}) = \Delta G^{\ddagger'}(L_\alpha \rightarrow H_{II}) + 2\kappa N_A N_{\text{coop}} A_n \{\beta^2 T^2 + D_1(T - T') - \beta^2 T' T\} \quad (10)$$

where

$$D_1 = 2C_1\beta + \beta^2 T' + 2C_1\alpha - 2\beta H_0 + 2\alpha\beta$$

As described in the Result section, we obtained the apparent activation energy by the slope of the curve of $\ln k$ vs $1/T$ as follows.

$$\frac{\partial \ln k}{\partial(1/T)} = -\frac{\Delta G^\ddagger}{R} + \frac{T}{R} \left(\frac{\partial \Delta G^\ddagger}{\partial T} \right) = -\frac{(\Delta G^{\ddagger'} - 2\kappa N_A N_{\text{coop}} A_n T' (\beta^2 T^2 + D_1))}{R} \quad (11)$$

Therefore, the apparent activation energy of the initial step, E_a ($L_\alpha \rightarrow H_{II}$), which was determined by the experimental results

shown in Figure 4a, is related to the theoretical activation energy, $\Delta G^{\ddagger'}(L_{\alpha} \rightarrow H_{II})$, as follows.

$$E_a(L_{\alpha} \rightarrow H_{II}) = \Delta G^{\ddagger'}(L_{\alpha} \rightarrow H_{II}) - 2\kappa N_A N_{\text{coop}} A_n T' / (\beta^2 T^2 + D_1) \quad (12)$$

To agree with the experimental results of the temperature dependence of k_1 , the value of $E_a(L_{\alpha} \rightarrow H_{II})$ must be constant, and hence $\beta = 0$ (i.e., the mean curvature of transition state $H^{\ddagger}(L_{\alpha} \rightarrow H_{II})$ is constant, $H^{\ddagger}(L_{\alpha} \rightarrow H_{II}) = C_1$). In this case, eq 12 can be converted to the following equation,

$$E_a(L_{\alpha} \rightarrow H_{II}) = \Delta G^{\ddagger'}(L_{\alpha} \rightarrow H_{II}) - 4\kappa N_A N_{\text{coop}} A_n \alpha T' / H^{\ddagger}(L_{\alpha} \rightarrow H_{II}) \quad (13)$$

Equation 13 can also be obtained from eq 9. We can reasonably consider that $H^{\ddagger}(L_{\alpha} \rightarrow H_{II})$ is negative if the stalk structure involves the transition state. In this case, $E_a(L_{\alpha} \rightarrow H_{II}) > \Delta G^{\ddagger'}(L_{\alpha} \rightarrow H_{II})$. If $H^{\ddagger}(L_{\alpha} \rightarrow H_{II}) \approx 0$, then $E_a(L_{\alpha} \rightarrow H_{II}) \approx \Delta G^{\ddagger'}(L_{\alpha} \rightarrow H_{II})$.

In contrast, values of the rate constant of the second step, k_2 , decreased with an increase in temperature for pH 2.6, although the k_2 values slightly increased with temperature at pH 2.7 and 2.8, and its analysis provides the values of $E_a(H_{II} \rightarrow Q_{II}^D)$ (Figure 4b). The former results indicate that $E_a(H_{II} \rightarrow Q_{II}^D)$ at pH 2.6 is negative. From the result of Figure 1c and the first-order approximation of temperature, we can consider that $H_{HII} = -C_2 - \beta T$, where C_2 and β are positive constants. We assume that the mean curvature of the transition state can be expressed similarly (i.e., $H^{\ddagger} = -C_3 - \gamma T$, where C_3 and γ are positive constants). Using eq 8, we can obtain the activation energy of this phase transition, $\Delta G^{\ddagger}(H_{II} \rightarrow Q_{II}^D)$, as follows.

$$\Delta G^{\ddagger}(H_{II} \rightarrow Q_{II}^D) = \Delta G^{\ddagger'}(H_{II} \rightarrow Q_{II}^D) + 2\kappa N_A N_{\text{coop}} A_n \left[\{(\alpha - \gamma)^2 - (\alpha - \beta)^2\} T^2 + 2\{(\alpha - \gamma)(C_0 - C_3) - (\alpha - \beta)(C_0 - C_2)\} T + D_2 \right]$$

where

$$D_2 = (C_0 - C_3)^2 - (C_0 - C_2)^2 - (H^{\ddagger'} - H_0')^2 + (H_A' - H_0')^2 = \text{const}$$

From the slope of the curve of $\ln k$ vs $1/T$, $E_a(H_{II} \rightarrow Q_{II}^D)$ can be obtained as follows.

$$E_a(H_{II} \rightarrow Q_{II}^D) = \Delta G^{\ddagger'}(H_{II} \rightarrow Q_{II}^D) + \{(\alpha - \beta)^2 - (\alpha - \gamma)^2\} T^2 + D_2 \quad (15)$$

To agree with the experimental results at pH 2.6 (i.e., the rate constant decreased with temperature), the value of $E_a(H_{II} \rightarrow Q_{II}^D)$ at pH 2.6 must be negative, and hence $(\alpha - \beta)^2 < (\alpha - \gamma)^2$. Generally, the absolute value of H_0 is larger than that of the H_{II} phase and the transition state. Therefore, $|\alpha - \beta| < |\alpha - \gamma|$. This indicates that the difference between the temperature dependence of the curvature of the transition state and H_0 is greater than that between that of the curvature of the initial state (i.e., the H_{II} phase) and H_0 . Therefore, as temperature increases, $\Delta G^{\ddagger}(H_{II} \rightarrow Q_{II}^D)$ increases greatly, and as a result the rate constant decreases with temperature. In contrast, to agree with the experimental results at pH 2.7 and 2.8 (i.e., the rate constant increased with temperature), the values of $E_a(H_{II} \rightarrow Q_{II}^D)$ at pH 2.7 and 2.8 must be constant, and hence $\beta = \gamma$. This indicates that the temperature dependence of the mean

curvature of the transition state is the same as that of the H_{II} phase at pH 2.7 and 2.8. This pH dependence may be explained by the change in the electrostatic interactions due to the surface charge density of the membrane.

It is instructive to describe the general relationship between ΔG^{\ddagger} and E_a of a phase transition. When $\Delta G^{\ddagger} = c$ (where c is a positive constant), $E_a = c$ (>0) and therefore the rate constant of the phase transition, k , increases with temperature, which can be applied to most cases. When $\Delta G^{\ddagger} = bT$ (where b is a positive constant), $E_a = 0$ and therefore k does not change with temperature. When $\Delta G^{\ddagger} = aT^2$ (where a is a positive constant), $E_a = -aT^2$ and therefore k decreases with temperature. When $\Delta G^{\ddagger} = aT^2 + bT + c$, $E_a = -aT^2 + c$ and therefore the sign of E_a depends on the values of a , c , and T .

Schöppe et al. obtained the apparent activation energies of the gel (L_{β}) to L_{α} phase transitions and the L_{β} to H_{II} phase transition of glycolipid membranes, which were 150–190 kJ/mol.⁵⁴ They considered that a specific number of lipid molecules (i.e., the number of molecules in a cooperative unit, N_{coop}) are involved in these phase transitions of lipid membranes cooperatively.^{35,54} Squires et al. determined the value of N_{coop} of the transition between the Q_{II}^G and Q_{II}^D phases³⁴ by the analysis of the results of the P -jump TR-SAXS experiments⁵⁵ using the data of the rate constant of the reverse transition; N_{coop} was $(3-6) \times 10^3$. This indicates that several thousand molecules undergo the $Q_{II}^G - Q_{II}^D$ phase transition cooperatively within one “cooperative unit”, which is equal to 1–2 unit cells of Q_{II}^G or 4–10 unit cells of Q_{II}^D .³⁵ In the present study, N_{coop} for both steps of the low-pH-induced L_{α} to Q_{II}^D phase transition in 20%-DOPS/80%-MO could not be determined. This phase transition was reversible; the addition of neutral buffer induced the phase transition from Q_{II}^D to L_{α} .¹⁷ However, we have not yet succeeded in measuring its rate constant of this reverse phase transition using the stopped flow apparatus because we could not get a uniform suspension of these cubic-phase membranes at low pH, which is essential for the stopped flow experiments.

It is instructive to consider other phase transitions where an intermediate H_{II} phase appeared. Squires et al. found the intermediate, transient H_{II} phase during the P -jump-induced Q_{II}^G to Q_{II}^D phase transition in a mixture of lauric acid and dilaurylphosphatidylcholine (2:1) from 600 to 240–360 bar at 50 wt % water.⁵⁶ The authors proposed a hypothesis that the intermediate H_{II} phase is a temporary “water donor” because the water content of the Q_{II}^D phase is larger than that of the Q_{II}^G phase at the phase transition. We tested this water donor hypothesis in our case (i.e., the low-pH-induced phase transition). We calculated the volume fraction of water, Φ_W , in each phase. (See the detailed calculation in the SI.) For the case of the 20%-DOPS/80%-MO membrane at pH 2.6 and 25 °C, Φ_W of the L_{α} , H_{II} , and Q_{II}^D phases are 0.66, 0.23, and 0.48, respectively. Therefore, it is difficult to apply the water donor hypothesis to the low-pH-induced L_{α} to Q_{II}^D phase transition. Cherezov et al. found in the temperature (T)-jump-induced L_{α} to Q_{II}^D phase transition in N -monomethylated dioleoylphosphatidylethanolamine (DOPE-Me) at a final temperature of 61 to 65 °C that a metastable H_{II} phase formed initially and disappeared very slowly while the Q_{II} phase developed; after 3 h of incubation, both phases coexisted.⁵⁷ The kinetic pathway for this system is similar to that of our DOPS/MO system, although the rate constant of the L_{α} to Q_{II}^D phase transition in our system is much larger than that of the T -jump transition in DOPE-Me. Recently, Siegel and Tenchov proposed to add the

unbinding energy of the L_{α} phase, g_w , to the free energy of each phase and succeeded in explaining the relative stability of each phase using their new theory; when g_u of the lipid membrane is small, then $T_{L \rightarrow Q}$ is lower than $T_{L \rightarrow H}$ and therefore the membrane exhibits the phase sequence $L_{\alpha} \rightarrow Q_{II} \rightarrow H_{II}$ as temperature increases (e.g., DOPE-Me), but when g_u is large, $T_{L \rightarrow Q}$ is greater than $T_{L \rightarrow H}$ and therefore a direct L_{α} to H_{II} phase transition occurs (i.e., the Q_{II} phase is metastable).⁴⁵ However, this theory cannot explain the appearance of the metastable H_{II} phase in the T-jump in DOPE-Me membranes.⁵⁷ On the other hand, when temperature increased at a heating rate of 1 °C/min in the DOPE-Me membrane, a direct L_{α} to H_{II} phase transition occurred without the formation of the Q_{II} phase.⁴⁵ This result indicates that $E_a(L_{\alpha} \rightarrow Q_{II}^D)$ of the DOPE-Me membrane is greater than its $E_a(L_{\alpha} \rightarrow H_{II})$. This is the same as for 20%-DOPS/80%-MO membranes at low pH.

5. CONCLUSIONS

In this study, we obtained the values and information on the activation energy of the elementary steps of the low-pH-induced L_{α} to Q_{II}^D phase transition in 20%-DOPS/80%-MO. The rate constant of the initial step increased with temperature, indicating that the value of $E_a(L_{\alpha} \rightarrow H_{II})$ does not change with temperature. Its analysis provided the values of $E_a(L_{\alpha} \rightarrow H_{II})$, which increased with an increase in pH. In contrast, the rate constant of the second step decreased with temperature for pH 2.6, although it increased with temperature at pH 2.7 and 2.8. These results indicate that the value of $E_a(H_{II} \rightarrow Q_{II}^D)$ at pH 2.6 increases with temperature, but the values of $E_a(H_{II} \rightarrow Q_{II}^D)$ at pH 2.7 and 2.8 are constant with temperature. The values of $E_a(H_{II} \rightarrow Q_{II}^D)$ were smaller than those of $E_a(L_{\alpha} \rightarrow H_{II})$ at the same pH. We analyzed these experimental results of the activation energies using a modified quantitative theory proposed initially by Squires et al.³⁵ The theory can reasonably explain these results qualitatively.

■ ASSOCIATED CONTENT

Supporting Information

The Supporting Information is available free of charge on the ACS Publications website at DOI: 10.1021/acs.langmuir.5b03785.

SAXS data of other conditions, waterfall plots of SAXS patterns, temperature dependence of the pH of membrane suspensions, correction of the activation energies based on the temperature-dependent pH shift, and calculation of the water content in each phase (PDF)

■ AUTHOR INFORMATION

Corresponding Author

*Tel/Fax: 81-54-238-4741. E-mail: yamazaki.masahito@shizuoka.ac.jp.

Notes

The authors declare no competing financial interest.

■ ACKNOWLEDGMENTS

This work was supported in part by a Grant-in-Aid for Scientific Research (B) (no. 15H04361) from the Japan Society for the Promotion of Science (JSPS) to M.Y. Part of this research is based on a Cooperative Research Project of the Research Institute of Electronics, Shizuoka University. The synchrotron radiation experiments were performed using BL40B2 at SPring-8 with the approval of the Japan Synchrotron Radiation

Research Institute (JASRI) (proposal nos. 2014A1180, 2014B1240, 2015A1242, and 2015B1208) and BL-6A of the Photon Factory (Tsukuba, Japan) with the approval of the Photon Factory Advisory Committee (proposal no. 2014G016). Preliminary SAXS experiments were performed at the Molecular Structure Analysis Section of Shizuoka University RIGST.

■ REFERENCES

- (1) Seddon, J. M.; Templer, R. H. Polymorphism of Lipid-Water Systems. Lipowsky, R., Sackmann, E., Eds.; In *Structure and Dynamics of Membranes*; Elsevier Science B. V.: Amsterdam, 1995; pp 97–160.
- (2) Luzzati, V. Biological significance of lipid polymorphism: the cubic phases. *Curr. Opin. Struct. Biol.* **1997**, *7*, 661–668.
- (3) Schwarz, U. S.; Gompper, G. Stability of inverse bicontinuous cubic phases in lipid-water mixtures. *Phys. Rev. Lett.* **2000**, *85*, 1472–1475.
- (4) Almsherqi, Z. A.; Kohlwein, S. D.; Deng, Y. Cubic membranes: a legend beyond the Flatland of cell membrane organization. *J. Cell Biol.* **2006**, *173*, 839–844.
- (5) Oka, T. Transformation between inverse bicontinuous cubic phases of a lipid from diamond to primitive. *Langmuir* **2015**, *31*, 3180–3185.
- (6) Aota-Nakano, Y.; Li, S. J.; Yamazaki, M. Effects of electrostatic interaction on the phase stability and structures of cubic phases of monoolein/oleic acid mixture membranes. *Biochim. Biophys. Acta, Biomembr.* **1999**, *1461*, 96–102.
- (7) Li, S. J.; Yamashita, Y.; Yamazaki, M. Effect of Electrostatic Interactions on Phase Stability of Cubic Phases of Membranes of Monoolein/Dioleoylphosphatidic Acid Mixture. *Biophys. J.* **2001**, *81*, 983–993.
- (8) Barriga, H. M. G.; Tyler, A. I. I.; McCarthy, N. L. C.; Parsons, E. S.; Ces, O.; Law, R. V.; Seddon, J. M.; Brooks, N. J. Temperature and pressure tuneable swollen bicontinuous cubic phases approaching nature's length scales. *Soft Matter* **2015**, *11*, 600–607.
- (9) Tyler, A. I. I.; Barriga, H. M. G.; Parsons, E. S.; McCarthy, N. L. C.; Ces, O.; Law, R. V.; Seddon, J. M.; Brooks, N. J. Electrostatic swelling of bicontinuous cubic lipid phases. *Soft Matter* **2015**, *11*, 3279–3286.
- (10) Angelov, B.; Angelova, A.; Drechsler, M.; Garamus, V. M.; Mutafchieva, R.; Lesieur, S. Identification of large channels in cationic PEGylated cubosome nanoparticles by synchrotron radiation SAXS and Cryo-TEM imaging. *Soft Matter* **2015**, *11*, 3686–3692.
- (11) Cherezov, V.; Clogston, J.; Misquitta, Y.; Abdel-Gawad, W.; Caffrey, M. Membrane protein crystallization in meso: lipid type-tailoring of the cubic phase. *Biophys. J.* **2002**, *83*, 3393–3407.
- (12) Chupin, V.; Killian, J. A.; de Kruijff, B. Effect of phospholipids and a transmembrane peptides on the stability of the cubic phase of monoolein: implication for protein crystallization from a cubic phase. *Biophys. J.* **2003**, *84*, 2373–2381.
- (13) Masum, S. M.; Li, S. J.; Tamba, Y.; Yamashita, Y.; Tanaka, T.; Yamazaki, M. Effect of de novo designed peptides interacting with the lipid-membrane interface on the stability of the cubic phases of the monoolein membrane. *Langmuir* **2003**, *19*, 4745–4753.
- (14) Masum, S. M.; Li, S. J.; Awad, T. S.; Yamazaki, M. Effect of Positively Charged Short Peptides on Stability of Cubic Phases of Monoolein/Dioleoylphosphatidic Acid Mixtures. *Langmuir* **2005**, *21*, 5290–5297.
- (15) Awad, T. S.; Okamoto, Y.; Masum, S. M.; Yamazaki, M. Formation of cubic phases from large unilamellar vesicles of dioleoylphosphatidylglycerol/monoolein membranes induced by low concentrations of Ca^{2+} . *Langmuir* **2005**, *21*, 11556–11561.
- (16) Yamazaki, M. Transformation between Liposomes and Cubic Phases of Biological Lipid Membranes Induced by Modulation of Electrostatic Interactions. *Adv. Planar Lipid Bilayers Liposomes* **2009**, *9*, 163–209.
- (17) Okamoto, Y.; Masum, S. M.; Miyazawa, H.; Yamazaki, M. Low pH-induced transformation of bilayer membrane into bicontinuous

cubic phase in dioleoyl-phosphatidylserine/monoolein membranes. *Langmuir* **2008**, *24*, 3400–3406.

(18) Pisani, M.; Fine, V.; Bruni, P.; Cola, E. D.; Francescangeli, O. Metal cation induced cubic phase in poly(ethylene glycol)-functionalized dioleoylphosphatidylethanolamine aqueous dispersions. *J. Phys. Chem. B* **2008**, *112*, 5276–5278.

(19) Silva, J. P. N.; Oliveira, R.; Coutinho, P. J. G. Characterization of mixed DODAB/monoolein aggregates using Nile Red as a solvatochromic and anisotropy fluorescent probe. *J. Photochem. Photobiol., A* **2009**, *203*, 32–39.

(20) Efrat, R.; Abramov, Z.; Aserin, A.; Garti, N. Nonionic-anionic mixed surfactants cubic mesophases. Part I: Structural chaotropic and kosmotropic effect. *J. Phys. Chem. B* **2010**, *114*, 10709–10716.

(21) Negrini, R.; Mezzenga, R. pH-responsive lyotropic liquid crystals for controlled drug delivery. *Langmuir* **2011**, *27*, 5296–5303.

(22) Muir, B. W.; Zhen, G.; Gunatillake, P.; Hartley, P. G. Salt induced lamellar to bicontinuous cubic phase transitions in cationic nanoparticles. *J. Phys. Chem. B* **2012**, *116*, 3551–3556.

(23) Oliveria, I. I. M. S. C.; Silv, J. P. N.; Feitos, E.; Marques, E. F.; Castanheira, E. M. S.; Oliveira, M. E. C. D. R. Aggregation behaviour of aqueous dioctadecyltrimethylammonium bromide/monoolein mixtures: A multitechnique investigation on the influence of composition and temperature. *J. Colloid Interface Sci.* **2012**, *374*, 206–217.

(24) Liu, Q.; Dong, Y.-D.; Hanley, T. L.; Boyd, B. J. Sensitivity of nanostructure in charged cubosomes to phase changes triggered by ionic species in solution. *Langmuir* **2013**, *29*, 14265–14273.

(25) Hartnett, T. E.; Ladewig, K.; O'Connor, A. J.; Hartley, P. G.; McLean, K. M. Size and phase control of cubic lyotropic crystal nanoparticles. *J. Phys. Chem. B* **2014**, *118*, 7430–7439.

(26) Liu, Q.; Wang, J.; Dong, Y.-D.; Boyd, B. J. Using a selective cadmium-binding peplipid to create responsive liquid crystalline nanomaterials. *J. Colloid Interface Sci.* **2015**, *449*, 122–129.

(27) Negrini, R.; Fong, W.-K.; Boyd, B. J.; Mezzenga, R. pH-responsive lyotropic liquid crystals and their potential therapeutic role in cancer treatment. *Chem. Commun.* **2015**, *51*, 6671–6674.

(28) Oka, T.; Tsuboi, T.; Saiki, T.; Takahashi, T.; Alam, J. M.; Yamazaki, M. Initial step of pH-jump-induced lamellar to bicontinuous cubic phase transition in dioleoylphosphatidylserine/monoolein. *Langmuir* **2014**, *30*, 8131–8140.

(29) Alam, M. M.; Oka, T.; Ohta, N.; Yamazaki, M. Kinetics of Low pH-Induced Lamellar to Bicontinuous Cubic Phase Transition in Dioleoylphosphatidylserine/Monoolein. *J. Chem. Phys.* **2011**, *134*, 145102.

(30) Seddon, J. M. Structure of the inverted hexagonal (H_{II}) phase, and non-lamellar phase transitions of lipids. *Biochim. Biophys. Acta, Rev. Biomembr.* **1990**, *1031*, 1–69.

(31) Shyamsunder, E.; Gruner, S. M.; Tate, M. W.; Turner, D. C.; So, P. T. C.; Tilcock, C. P. S. Observation of inverted cubic phases in hydrated dioleoylphosphatidylethanolamine membranes. *Biochemistry* **1988**, *27*, 2332–2336.

(32) Koynova, R.; Caffrey, M. Phase and phase-transitions of the hydrated phosphatidylethanolamines. *Chem. Phys. Lipids* **1994**, *69*, 1–34.

(33) Marrink, S.-J.; Tieleman, D. P. Molecular dynamics simulation of spontaneous membrane fusion during a cubic-hexagonal phase transition. *Biophys. J.* **2002**, *83*, 2386–2392.

(34) Siegel, D. P.; Kozlov, M. M. The Gaussian curvature elastic modulus of N-monomethylated dioleoylphosphatidylethanolamine; relevance to membrane fusion and lipid phase behaviour. *Biophys. J.* **2004**, *87*, 366–374.

(35) Squires, A. M.; Conn, C. E.; Seddon, J. M.; Templer, R. H. Quantitative model for the kinetics of lyotropic phase transitions involving changes in monolayer curvature. *Soft Matter* **2009**, *5*, 4773–4779.

(36) Bartlett, G. R. Phosphorous assay in column chromatography. *J. Biol. Chem.* **1959**, *234*, 466–468.

(37) Paatero, P.; Tapper, U. Positive matrix factorization: A non-negative factor model with optimal utilization of error estimates of data values. *Environmetrics* **1994**, *5*, 111–126.

(38) Wang, J.-H.; Hopke, P. K.; Hancewicz, T. M.; Zhang, S. L. Application of modified alternating least squares regression to spectroscopic image analysis. *Anal. Chim. Acta* **2003**, *476*, 93–109.

(39) Qiu, H.; Caffrey, M. The phase diagram of the monoolein/water system: metastability and equilibrium aspects. *Biomaterials* **2000**, *21*, 223–234.

(40) Tate, M. W.; Gruner, S. Temperature dependence of the structural dimensions of the inverted hexagonal (H_{II}) phase of phosphatidylethanolamine-containing membranes. *Biochemistry* **1989**, *28*, 4245–42894253.

(41) Marsh, D. Intrinsic curvature in normal and inverted lipid structures and in membranes. *Biophys. J.* **1996**, *70*, 2248–2255.

(42) Kinoshita, K.; Li, S. J.; Yamazaki, M. The mechanism of the stabilization of the hexagonal II (H_{II}) phase in phosphatidylethanolamine membranes in the presence of low concentrations of dimethyl sulfoxide. *Eur. Biophys. J.* **2001**, *30*, 207–220.

(43) Schwarz, U. S.; Gompper, G. Stability of inverse bicontinuous cubic phases in lipid-water mixtures. *Phys. Rev. Lett.* **2000**, *85*, 1472–1475.

(44) Schwarz, U. S.; Gompper, G. Bending frustration of lipid-water mesophases based on cubic minimal surfaces. *Langmuir* **2001**, *17*, 2084–2096.

(45) Siegel, D. P.; Tenchov, B. G. Influence of the lamellar phase unbinding energy on the relative stability of lamellar and inverted cubic phases. *Biophys. J.* **2008**, *94*, 3987–3995.

(46) Barriga, H. M. G.; Tyler, A. I. I.; McCarthy, N. L. C.; Parsons, E.; Ces, O.; Law, R. V.; Seddon, J. M.; Brooks, N. J. Temperature and pressure tuneable swollen bicontinuous cubic phases approaching nature's length scales. *Soft Matter* **2014**, *11*, 600–607.

(47) Siegel, D. P.; Epand, R. M. The mechanism of lamellar-to-inverted hexagonal phase transitions in phosphatidylethanolamine: implications for membrane fusion mechanisms. *Biophys. J.* **1997**, *73*, 3089–3111.

(48) Siegel, D. P. The modified stalk mechanism of lamellar/inverted phase transitions and its implications for membrane fusion. *Biophys. J.* **1999**, *76*, 291–313.

(49) Karal, M. A. S.; Yamazaki, M. Activation energy of tension-induced pore formation in lipid membranes. *J. Chem. Phys.* **2015**, *143*, 081103.

(50) Karal, M. A. S.; Levadny, V.; Tsuboi, T.; Belaya, M.; Yamazaki, M. Electrostatic interaction effects on tension-induced pore formation in lipid membranes. *Phys. Rev. E* **2015**, *92*, 012708.

(51) Helfrich, W. Elastic properties of lipid bilayers: theory and possible experiments. *Z. Naturforsch., C* **1973**, *28*, 693–703.

(52) Strey, R. Microemulsion microstructure and interfacial curvature. *Colloid Polym. Sci.* **1994**, *272*, 1005–1019.

(53) Templer, R. H.; Seddon, J. M.; Duesing, P. M.; Winter, R.; Erbes, J. Modeling the phase behaviour of the inverse hexagonal and inverse bicontinuous cubic phases in 2:1 fatty acid/phosphatidylcholine mixture. *J. Phys. Chem. B* **1998**, *102*, 7262–7271.

(54) Schöppe, A.; Hinz, H. - J.; Gerdes, R.; Redlich, H.; Rapp, G. Activation energies and kinetics of glycolipid phase transitions. *Chem. Phys. Lipids* **1999**, *103*, 95–115.

(55) Conn, C. E.; Ces, O.; Squires, A. M.; Mulet, X.; Winter, R.; Finet, S. M.; Templer, R. H.; Seddon, J. M. A pressure-jump time-resolved X-ray diffraction study of cubic-cubic transition kinetics in monoolein. *Langmuir* **2008**, *24*, 2331–2340.

(56) Squires, A. M.; Templer, R. H.; Seddon, J. M.; Woenckhaus, J.; Winter, R.; Narayanan, T.; Finet, S. Kinetics and mechanism of interconversion of inverse bicontinuous cubic mesophase. *Phys. Rev. E* **2005**, *72*, 011502.

(57) Cherezov, V.; Siegel, D. P.; Shaw, W.; Burgess, S. W.; Caffrey, M. The kinetics of non-lamellar phase formation in DOPE-Me: relevance to biomembrane fusion. *J. Membr. Biol.* **2003**, *195*, 165–182.